Evidence for the involvement of Fibroblast Growth Factor 10 in lipofibroblast formation during embryonic lung development

Denise Al Alam[1]*, Elie El Agha[2]*, Reiko Sakurai[3], Vahid Kheirollahi[2], Alena Moiseenko[2], Soula Danopoulos[1], Amit Shrestha[2], Carole Schmoldt[2], Jennifer Quantius[2], Susanne Herold[2], Cho-Ming Chao[2], Caterina Tiozzo[4], Stijn De Langhe[5], Maksim V. Plikus[6], Matthew Thornton[8], Brendan Grubbs[8], Parviz Minoo[9], Virender K. Rehan[3#] and Saverio Bellusci[1,2,7#]

[1] Department of Surgery, Saban Research Institute of Children's Hospital Los Angeles, Los Angeles, CA 90027, USA.

[2] Excellence Cluster Cardio-Pulmonary System, Universities of Giessen and Marburg Lung Center. Member of the German Center for Lung Research. Department of Internal Medicine II, Klinikstrasse 36, 35392 Giessen, Hessen, Germany.

[3] Department of Pediatrics, Los Angeles Biomedical Research Institute at Harbor-UCLA, Torrance, CA 90502, USA.

[4] Division of Neonatology, Department of Pediatrics, Columbia University, New York, NY, USA.

[5] Department of Pediatrics, Division of Cell Biology, National Jewish Health, Denver, CO 80206, USA.

[6] Department of Developmental and Cell Biology, Sue and Bill Gross Stem Cell Research Center, Center for Complex Biological Systems, University of California Irvine, Irvine, CA 92697, USA.

[7] Institute of Fundamental Medicine and Biology, Kazan Federal University, Kazan, Russia.

[8] Maternal Fetal Medicine Division, University of Southern California, Los Angeles, CA, 90033

[9] Division of Neonatal Medicine, University of Southern California, Los Angeles, CA, 90033

Key words: Fgf10, lipofibroblasts, lung, mesenchyme

*: Equal contribution

#: Co-corresponding authors:

Saverio Bellusci: Excellence Cluster Cardio-Pulmonary System, Universities of Giessen and Marburg Lung Center. Member of the German Lung Center. Department of Internal Medicine II, Klinikstrasse 36, 35392 Giessen, Germany. Tel: 49 (0) 641 99 46 730, email: Saverio.Bellusci@innere.med.uni-giessen.de

Virender K Rehan: Department of Pediatrics, Los Angeles Biomedical Research Institute at Harbor-UCLA, Torrance, CA 90502, USA. Tel: 3102221965; email: vrehan@labiomed.org

Abstract

Lipid-containing alveolar interstitial fibroblasts, or simply lipofibroblasts, are increasingly recognized as an important component of the epithelial stem-cell niche in the rodent lung. Although lipofibroblasts were initially believed to merely assist type 2 alveolar epithelial cells in surfactant production during neonatal life, recent evidence suggests that these cells are indispensable for the survival and growth of epithelial stem cells during adult life. Despite the increasing interest in lipofibroblast biology, little is known about their cellular origin or the molecular pathways controlling their formation during embryonic development. Here, we show that a population of lipid-droplet-containing stromal cells emerges in the developing mouse lung between E15.5 and E16.5. This event is accompanied by significant upregulation, in the lung mesenchyme, of peroxisome proliferator-activated receptor gamma (the master switch of lipogenesis), adipose differentiation-related protein (marker of mature lipofibroblasts) and fibroblast growth factor 10 (previously shown by our group to identify a subpopulation of lipofibroblast progenitors). We also demonstrate that although only a subpopulation of total embryonic lipofibroblasts derives from *Fgf10*-positive progenitor cells, *in vivo* knockdown of Fgfr2b ligand activity as well as reduction in *Fgf10* expression lead to global reduction in the expression levels of lipofibroblast markers at E18.5. Constitutive *Fgfr1b* knockouts and mutants with conditional partial inactivation of *Fgfr2b* in the lung mesenchyme reveal the involvement of both receptors in lipofibroblast formation and suggest a possible compensation between the two receptors. We also provide data from human fetal lungs to demonstrate the relevance of our discoveries to humans. Our results reveal an essential role for Fgf10 signaling in the formation of lipofibroblasts during late lung development.

Introduction

Lipofibroblasts (LIFs) are lipid droplet-containing interstitial fibroblasts that are located within close proximity to type 2 alveolar epithelial cells (AECII) (McGowan and Torday, 1997; O'Hare and Sheridan, 1970). LIFs contribute to the production of pulmonary surfactant by assimilating neutral lipids and transferring them to AECII for final processing of the surfactant. They also contain retinoic acids that are essential for the promotion of postnatal alveolar septation, a critical process that increases blood/gas exchange surface (Simon and Mariani, 2007). LIFs are detected in the embryonic rat lung starting at embryonic day 16 (E16) and their numbers increase afterwards, peaking during the second postnatal week when alveologenesis is at its peak (Tordet et al., 1981). Although LIFs have been studied in postnatal lungs, their exact cellular origin and mechanism of differentiation remain unknown.

LIFs are present in adult human and mouse lungs (Kaplan et al., 1985; Rehan et al., 2006). *In vitro* models of LIF differentiation from mesenchymal progenitors, using either the human embryonic lung fibroblast cell line (WI-38) or neonatal and adult human lung biopsies have helped establish some of the critical regulators of LIF differentiation (Rehan et al., 2006). Previous reports have shown that *Thy1*-positive, but not *Thy1*-negative cells are able to acquire LIF characteristics such as lipid-droplet accumulation and collagen formation shortly after *in vitro* culture (Penney et al., 1992). Recently, it has been proposed that LIFs could contribute to the AECII stem-cell niche in the adult lung (Barkauskas et al., 2013).

LIFs share common characteristics with adipocytes and it is already established that peroxisome proliferator-activated receptor gamma (Pparg), the master regulator of adipogenesis, is also required for the maintenance of the LIF phenotype (Torday et al., 2003). In LIFs, Pparg is downstream of parathyroid hormone-related protein (Pthrp) signaling and it has been shown that *in vivo* inactivation of the Pthrp pathway leads to abnormal alveolarization with defective surfactant synthesis (Rubin et al., 2004). Following Pparg activation, LIFs express adipose differentiation-related protein (Adrp), a trafficking protein that escorts lipid substrates within the LIF cytosol and delivers them to adjacent AECII (Schultz et al., 2002).

Fibroblast growth factor 10 (*Fgf10*) is expressed by both pre- and mature adipocytes, and plays an important role in the differentiation of pre-adipocytes in the white adipose tissue via the activation of the Pparg pathway (Sakaue et al., 2002). Interestingly, Fgf10 also stimulates cell proliferation in white adipose tissue (Konishi et al., 2006) and *Fgf10*-null embryos display impaired white adipose tissue formation (Asaki et al., 2004; Mailleux et al., 2002). A recent study demonstrated that P8 mouse lipofibroblasts expressing low levels of platelet derived growth factor receptor alpha (*Pdgfra*), express high levels of *Fgf10* and its receptors *Fgfr1b* and *Fgfr2b* (McGowan and McCoy, 2015). Using the *Fgf10*^{iCre} lineage-tracing tool (El Agha et al., 2012), we have shown that *Fgf10*-positive cells are progenitors for LIFs, among other lineages, in the developing mouse lung (El Agha et al., 2014). Based on that and extrapolating our knowledge about the role of Fgf10 in adipocytes to pulmonary LIFs, we hypothesized that Fgf10 signaling plays an important role in the formation of pulmonary LIFs. To our knowledge, there are currently no reported studies on the role of Fgf10 signaling in the formation of LIFs.

To test our hypothesis, enhancer-trap, transgenic and knock-in mouse lines were used to identify the *Fgf10*-expressing lipofibroblast subpopulation and to study the consequences of disrupting Fgf10 signaling on overall LIF formation in the developing mouse lung. The impact of mesenchymal *Fgfr2b* deletion as well as the ubiquitous *Fgfr1b* deletion on LIF formation was investigated, the results of which suggest that Fgfr2b compensates for the loss of Fgfr1b. The effect of recombinant FGF10 protein on mouse and human fetal lung mesenchymal cells was also tested. Taken together, our results demonstrate a novel role for mesenchymal Fgf10 signaling in the formation of LIFs.

Results

Lipofibroblast formation progressively increases during embryonic lung development

Since the emergence of LIFs in the embryonic mouse lung was unexplored, we first quantified the relative number of lipid droplet-containing cells between E13.5 and E18.5 by LipidTOX staining followed by Fluorescence Activated Cell Sorting (FACS). LipidTOX is a dye that labels neutral lipids that are abundantly present in LIFs. Our results indicated that LipidTOX-positive cells emerge between E15.5 and E16.5 and they represented up to 30% of the total cell count in the developing lung (Fig. 1A,B). Next, the expression levels of *Adrp*, *Pparg* and *Fgf10* were examined throughout lung development by qPCR (Fig. 1C). *Adrp* expression showed very low levels between E11.5 to E15.5 and was upregulated beginning at E16.5, and peaked at E18.5. *Pparg* expression was first detected at E15.5 and increased progressively up to E18.5. *Fgf10* expression increased steadily from E11.5 to E18.5.

Following tamoxifen IP injection of *Fgf10*$^{iCre/+}$*; tomato*$^{flox/+}$ mice at E11.5 or E15.5, around 30% and 40% of labeled cells, respectively, trace to *Adrp*-positive LIFs when quantified at E18.5 (El Agha et al., 2014). In this study, double tamoxifen IP labeling was carried out at E11.5 and E14.5 in order to maximize the labeling of LIFs derived from *Fgf10*-positive cells (Fig. 1D). Immunofluorescence staining (IF) for Adrp on the resulting E18.5 lungs showed that only a small proportion of *Adrp*-positive cells are also RFP-positive (Fig. 1E). However, quantification of IF indicated that around 65% of the RFP-positive cells are *Adrp*-positive (Fig. 1F) demonstrating the increased efficiency of our double tamoxifen IP approach to mark *Fgf10*-positive LIFs. LipidTOX staining followed by FACS analysis was also used to confirm these data. Our data indicated that RFP-positive cells represent around 4% of the total lung cells, of which 66.5% are also LipidTOX-positive (Fig. 1H). The same analysis showed that 8.37% of total LipidTOX-positive cells are RFP-positive at E18.5 (Fig. 1G).

Next, we used the previously reported *Fgf10-lacZ* enhancer-trap mouse line to monitor *Fgf10* expression during neonatal life, and showed that a subset of *Fgf10*-positive cells displays LIF characteristics at P5 (Adrp-positive, Oil Red O (ORO)-positive) (Fig. S1). The Adrp/ LacZ double positive cells represented around 27% of

total LIFs at this stage. In conclusion, *Fgf10*-expressing cells and their descendants represent only a fraction of the total LIF population in the developing mouse lung. In order to test whether Fgf10 signaling is involved in LIF formation, we used two independent but complementary approaches: attenuation of Fgfr2b signaling and generation of *Fgf10* hypomorphic lungs.

Attenuation of Fgfr2b ligand activity leads to impaired lipofibroblast formation

To attenuate Fgfr2b ligand activity, we used our previously reported and validated double transgenic (DTG) system to overexpress a soluble form of Fgfr2b in a ubiquitous fashion in the embryo upon doxycycline exposure (Parsa et al., 2010; Parsa et al., 2008; Volckaert et al., 2011). Soluble Fgfr2b acts as a decoy receptor to block all Fgfr2b ligands, including Fgf10, potentially expressed at the time of doxycycline administration. Based on the expression pattern of LIF markers and the LipidTOX staining during lung development (Fig. 1B,C), doxycycline was administered between E14.5 and E18.5 to attenuate Fgfr2b ligand activity (Fig. 2A). Compared to control lungs (n=4), DTG lungs (n=4) were smaller (Fig. 2C vs. B) and displayed dilated distal airways and thickened mesenchyme (Fig. 2E vs. D), indicating an arrest in overall lung development. Adrp IF and ORO staining showed a decrease in Adrp expression (Fig. 2H,I vs. F,G) and lipid-droplet content (Fig. 2L,M vs. J,K) in DTG compared to control lungs. The observed decrease in Adrp expression and ORO staining was validated by qPCR. DTG lungs display a clear reduction in the expression levels of *Pparg* (Fig. 2N; P<0.01) and *Adrp* (Fig. 2O; P<0.001) compared to control lungs. The decrease in Pparg expression was also observed at the protein level as shown by western blotting (Fig. 2P).

***Fgf10* hypomorphs display impaired lipofibroblast formation**

As a second approach, the impact of decreased *Fgf10* expression on LIF formation during lung development was investigated. Since the complete deletion of *Fgf10* leads to lung agenesis (Sekine et al., 1999), the *Fgf10* hypomorphic allele was used (Mailleux et al., 2005; Ramasamy et al., 2007) to generate E18.5 $Fgf10^{iCre/+}$; $tomato^{flox}$ (control) and $Fgf10^{iCre/lacZ}$; $tomato^{flox}$ (hypomorph) lungs (Fig. 3A). $Fgf10^{iCre}$ allele is phenotypically equivalent to the *Fgf10*-null allele (El Agha et al., 2012). This experimental setup allows studying the impact of decreased *Fgf10*

expression on global LIF formation (paracrine/autocrine effects of Fgf10) as well as the impact of decreased *Fgf10* expression on the contribution of *Fgf10*-expressing cells to total LIFs (autocrine effect of Fgf10).

Impaired hindlimb development was observed in $Fgf10^{iCre/lacZ}$; $tomato^{flox}$ embryos thus validating phenotypically the reduced *Fgf10* expression (data not shown). $Fgf10^{iCre/lacZ}$ experimental lungs were smaller, lacked the accessory lobe (arrow in Fig. 3C vs. B) and displayed thicker intersaccular walls as well as hemorrhagic areas upon histological analysis (data not shown). Gene expression analysis revealed a significant decrease in *Fgf10* expression (Fig. 3F; $P<0.01$) in hypomorphic lungs ($n=3$) compared to littermate controls ($n=3$). qPCR also showed a significant reduction in the expression levels of *Pparg* (Fig. 3G; $P<0.05$) and *Adrp* (Fig. 3H; $P<0.05$) in hypomorphic lungs compared to littermate controls.

Immunofluorescence for Adrp showed that hypomorphic lungs exhibit a global decrease in Adrp expression compared to controls (Fig. 3K,L vs. I,J). Quantification of the Adrp signal using MetaMorph software revealed a significant decrease in the number (Fig. 3M; $P<0.05$) and area (Fig. 3N; $P<0.05$) of Adrp immunoreactive spots in hypomorphic lungs ($n=3$) compared to littermate controls ($n=3$).

The $Tomato^{flox}$ reporter allele was introduced in the background of $Fgf10^{iCre/+}$ (control) and $Fgf10^{iCre/lacZ}$ (hypomorph) embryos to label *Fgf10*-positive cells at E14.5 with a single tamoxifen IP injection (Fig. 3A,D,E) allowing the investigation of the autocrine effect of Fgf10. Lineage-labeled cells in the background of Adrp IF do not display any significant difference between control and hypomorph lungs in terms of Adrp spot number (Fig. 3S; $P=0.2568$). However, we observed a significant decrease in the area of Adrp immunoreactive spots (Fig. 3T; $P<0.05$) in the hypomorphs ($n=3$) compared to controls ($n=3$) (Fig. 3Q,R vs. O,P). These data suggest a defect in lipid droplet formation resulting in impaired LIFs differentiation.

Fgf10 acts on the mesenchyme to induce lipofibroblast formation

In order to rule out any contribution from the epithelium to LIF formation and to demonstrate a direct effect for Fgf10 on mesenchymal cells, primary lung mesenchyme was cultured at different embryonic stages (E14.5-E18.5). Following differential adhesion, unattached cells were washed and mesenchymal cells were

allowed to grow for 24 h before RNA isolation (Fig. 4A). The cells remaining in the primary culture consist of a heterogeneous population of mesenchymal cells. In cultures derived from E18.5 lungs, lipofibroblasts represented about only one third of the total adherent cells (Fig. S2). Fig. 4B shows representative images for Cdh1 IF performed on primary mesenchymal cells, indicating minimal epithelial contamination. qPCR revealed low expression levels for *Pparg* (Fig. 4D) and *Adrp* (Fig. 4E) at E14.5 and E15.5 and then increased expression levels between E16.5 and E18.5. This is consistent with the data obtained with lung homogenates (Fig. 1C), thus indicating upregulation of *Pparg* and *Adrp* in the lung mesenchyme during late embryonic stages. Parallel to the increase in LIF markers, *Fgf10* expression was also increased in late embryonic stages (Fig. 4C). Strikingly, *Fgfr2b* and *Fgfr1b*, the genes encoding the two Fgf10 receptors, were upregulated in late embryonic lung mesenchyme with the increase in *Fgfr2b* expression preceding that observed for *Fgfr1b* (Fig. 4F,G).

In order to demonstrate a direct effect for Fgf10 on mesenchymal cells, primary mesenchymal cultures of E19 rat lungs were treated with recombinant human (rh)FGF10. ORO staining after 24 h revealed a significant increase in the number of lipid-droplet-containing cells upon rhFGF10 treatment (Fig. 4I vs. H; J; $P<0.05$). When treated with increasing concentrations of rhFGF10, these cells showed a dose-dependent increase in Pparγ as detected by Western blotting (Fig. 4K,L; $P<0.05$).

Analysis of *Fgfr1b*-null lungs suggests a compensatory role for *Fgfr2b* in lipofibroblast formation

Given the observed sequential expression of *Fgfr2b* and *Fgfr1b* in the lung mesenchyme (Fig. 4F,G), we tested whether Fgf10 signaling in the mesenchyme via these receptors is involved in LIF formation. First, the phenotype of E18.5 *Fgfr1b* knockout lungs was carried out and analysis by qPCR confirmed the absence of *Fgfr1b* expression in knockout lungs ($n=4$) compared to control lungs ($n=7$) (Fig. 5A; $P<0.01$). H&E staining did not show any apparent phenotype in knockout lungs compared to control lungs (Fig. 5H,I vs. F,G). Interestingly, qPCR analysis showed that *Pparg* is significantly increased in the knockouts compared to controls (Fig. 5C; $P<0.01$), and this was accompanied with a modest increase in *Adrp* expression (Fig.

5D; *P*=0.4762). Surprisingly, *Fgfr2b* expression is increased (Fig. 5E; *P*<0.01); whereas *Fgf10* expression levels remain unchanged (Fig. 5B; *P*=4082).

The expression levels of Adrp were also investigated at the protein level by IF. The staining revealed a slight increase in Adrp immunoreactivity in the knockouts (Fig. 5L,M) compared to controls (Fig. 5J,K). Quantification of the Adrp signal using MetaMorph software showed a trend towards an increase in the number (Fig. 5N; *P*=0.0629) and area (Fig. 5O; *P*=0.2921) of Adrp immunoreactive spots in knockout lungs (*n*=3) compared to control lungs (*n*=3).

Our results therefore indicate that ubiquitous deletion of *Fgfr1b* in the lung does not compromise LIF formation during embryonic development; rather trends towards increasing LIF formation. Interestingly, the elevated levels of *Fgfr2b* in *Fgfr1b* knockout lungs suggest that *Fgfr2b* could be compensating for the loss of *Fgfr1b*, thereby allowing normal, and even enhanced LIF formation.

Partial loss of mesenchymal *Fgfr2b* expression impairs lipofibroblast formation

We showed so far that *Fgfr2b* is expressed in mesenchymal cells and that Fgf10 acts directly on mesenchymal cells to promote LIF formation. To test whether mesenchymal Fgfr2b signaling plays a role in LIF formation *in vivo*, we carried out a partial loss of *Fgfr2b* expression in the lung mesenchyme. Conditional genetic deletion of *Fgfr2b* in the lung mesenchyme was achieved by injecting female mice carrying *Tg(Tbx4-LMECreERT2)/+; fgfr2b*$^{+/+}$ (control) and *Tg(Tbx4-LMECreERT2)/+; fgfr2b*$^{flox/+}$ (mutant) embryos with tamoxifen at E14.5. The lungs from mutant embryos are therefore expected to exhibit a 50% decrease in *Fgfr2b* expression in the mesenchyme only. The recombination of the *Fgfr2b*^{flox} allele in E18.5 mutant lungs was validated by PCR (Fig. 6A). No major phenotypic differences were observed between mutant and control lungs at E18.5 (Fig. 6D,E vs. B,C). However, qPCR analysis indicated a trend towards decreased *Fgfr2b* expression (Fig. 6F; *P*=0.0995). A statistically significant reduction in *Adrp* expression was demonstrated (Fig. 6G; *P*<0.05), suggesting defective LIF formation in mutant lungs (*n*=5) compared to control lungs (*n*=3). However, no significant differences were observed in the expression levels of Pparg (Fig. 6H; *P*=0.2591) or Spry4 (as a readout for mesenchymal Fgf signaling) (Fig. 6I; *P*=0.9291).

Immunofluorescence for Adrp was also carried out and the results indicated a decrease in Adrp staining in mutant lungs (Fig. 6L,M) compared to control lungs (Fig. 6J,K). Quantification of the Adrp signal using MetaMorph software revealed a trend towards decreased number (Fig. 6N; P=0.1037) and area (Fig. 6O; P=0.1716) of Adrp immunoreactive spots in mutant lungs (n=5) compared to control lungs (n=3).

Our results therefore indicate that deletion of one *Fgfr2b* allele in the lung mesenchyme starting at E14.5 impairs the LIF status at E18.5 at the RNA level and to a lesser extent at the protein level.

Relevance of lipofibroblast formation in mice to human lungs

In order to demonstrate the relevance of our findings to human lungs, the expression levels of *FGF10* and *ADRP* were analyzed in human fetal lung homogenates between weeks 10 and 21 of gestation ($3 \leq n \leq 11$ for each time point). Our human data show significant increase in *FGF10* only between 10 and 18 weeks of gestation (Fig. 7A) while in mouse *Fgf10* expression rises constantly throughout lung development (Fig. 1C). Our results also indicate that *ADRP* expression is unchanged between 10 and 21 weeks of gestation (Fig. 7B). Interestingly, the start of *Adrp* expression in mouse was seen between E15.5 and E16.5 (Fig. 1C) corresponding to weeks 20 and 22 of gestation. These data suggest that LIF formation in human lungs likely occurs past week 22, corresponding to the mid-canalicular stage of lung development.

Using the human embryonic lung fibroblast cell line (WI-38), we show that treatment with rhFGF10 leads to a significant increase in the number of lipid-droplet-containing cells (Fig. 7D vs. C; E; n=3; P<0.05). Triolein uptake assay demonstrated increased lipogenesis in WI-38 cells treated with increasing concentrations of rhFGF10 (Fig. 7F; P<0.05). Finally, treating WI-38 cells with increasing concentrations of rhFGF10 also led to a dose-dependent increase in PPARg (Fig. 7G), thus reinforcing the proposed role of mesenchymal FGF10 signaling in LIF formation. Lastly, epithelial and mesenchymal cells were isolated from fetal human lungs at 16 weeks gestational stage and RNA was isolated. Gene expression analysis showed an enrichment of *FGF10* and *FGFR1b* expression in the mesenchymal fraction while *FGFR2b* was enriched in the epithelial fraction (Fig. 7H-J; n=2).

Discussion

Although pulmonary LIFs were first described in the 1970s and extensively studied in rodents, their lineage origin and molecular pathways leading to their formation are still unknown. Previously, we utilized *Fgf10-lacZ* mice to show that during early embryonic lung development (E12.5-E13.5), *Fgf10* expression identifies airway smooth muscle cell (SMC) progenitors (Mailleux et al., 2005). More recently, using *Fgf10*^{iCre} knock-in mice, we showed that during late pseudoglandular and early saccular stages (E15.5-E18.5), *Fgf10* is predominantly expressed in cells of the lung parenchyma compared to the airway SMCs and these cells are mostly identified as LIFs (El Agha et al., 2014). Here, we provide evidence that Fgf10 plays a functional role in LIF formation.

LIFs and adipocytes share many aspects of their terminal differentiation program, known as lipogenesis. However, it is currently unknown whether the similarities between LIFs and adipocytes extend into earlier stages of lineage formation. Our current findings provide new evidence that LIF formation depends on Fgf10 signaling and this parallels Fgf10-dependency of white adipose tissue formation, reported earlier (Asaki et al., 2004; Sakaue et al., 2002). Interestingly, the role of the autocrine/paracrine effect of Fgf10, acting through Fgfr2b, in the development of the white adipose tissue has already been suggested (Ohta and Itoh, 2014). Here, we demonstrate that Fgf10 also signals in an autocrine/paracrine fashion in another mesenchymal and adipocyte-like cell type, the pulmonary LIF.

Fgf10 expression identifies a distinct subset of pulmonary lipofibroblasts

Our data identify a previously unappreciated heterogeneity of pulmonary LIFs. Based on our results, LIFs consist of *Fgf10*-positive and *Fgf10*-negative subpopulations.

Previously, we reported that in *Fgf10*^{iCre} mice, the partial deletion of transcription factor binding sites located in intron 1 of the *Fgf10* gene led to decreased Cre expression compared to the endogenous *Fgf10* expression (El Agha et al., 2012). Thus, the possibility that *Fgf10*-negative LIFs reflect inefficient labeling of *Fgf10*-positive cells cannot be excluded. However, since *lacZ*-negative LIFs are also found in *Fgf10-lacZ* lungs, we deduce that there are at least two LIF sources in the embryonic lung, partly distinguishable by *Fgf10* expression.

The difference between these two pools (*Fgf10*-positive and *Fgf10*-negative LIFs) in terms of origin and fate is unclear. In addition, a critical question remains open: what are the other endogenous factors contributing to LIF lineage specification and maturation? For example, it has been shown that lung *Thy1*-positive cells differentiate into LIFs through activation of Pparg while *Thy1*-negative cells differentiate into myofibroblasts (McIntosh et al., 1994; Phipps et al., 1990; Varisco et al., 2012). Pparg signaling is one of the major pathways, described to date, involved in the differentiation of LIFs (Ferguson et al., 2009; McGowan and Torday, 1997). In addition, *ex vivo* studies of human and mouse tissues suggest that endothelial cells within the developing adipose tissue can give rise to mature adipocytes (Tran et al., 2012), although this has been recently contested (Berry and Rodeheffer, 2013). The use of lineage-specific labeling for Thy1 and endothelial cells in the background of $Fgf10^{iCre/+}$; $tomato^{flox/+}$ would help identify whether these are distinct cell populations capable of giving rise to LIFs.

Fgf10 plays a critical role in lipofibroblast formation

The overexpression of a dominant negative decoy receptor for Fgfr2b ligands demonstrated that Fgfr2b ligands are critical for LIF formation during late lung development. In addition to *Fgf10*, *Fgf1* and *Fgf7* are the two other Fgfr2b ligands expressed in the developing lung (Bellusci et al., 1997). Contrary to Fgf10, which binds Fgfr2b and Fgfr1b, Fgf7 binds only to Fgfr2b while Fgf1 binds to all Fgf receptors (Ornitz et al., 1996). *Fgf7*-null mice are viable and display impaired hair and kidney development (Guo et al., 1996; Qiao et al., 1999) while *Fgf1*-null mice develop enlarged adipocytes and inflammation of the adipose tissue only after a high fat diet (Jonker et al., 2012). It remains possible that Fgf1 and Fgf7 signaling could also contribute to LIF formation. However, the data obtained with the *Fgf10* hypomorphs strongly suggest a combined autocrine and paracrine mode for Fgf10 signaling during LIF formation since both LIF subpopulations (*Fgf10*-positive and *Fgf10*-negative) are adversely affected by decreased *Fgf10* expression. A recent study suggested an autocrine role for Fgf10 signaling in promoting lipid storage in LIFs, but with no evidence of such signaling (McGowan and McCoy, 2015). Considering many similarities between LIFs and adipocytes and given the known role of Fgf10 in adipogenesis, it is reasonable to draw parallels between adipocytes and LIFs.

Fgfr1b and Fgfr2b play redundant roles in the mesenchyme as receptors for Fgf10

Fgfr2b is the main Fgf10 receptor as demonstrated by phenotypical similarities between *Fgfr2b*-null pups (De Moerlooze et al., 2000) and *Fgf10*-null pups (Sekine et al., 1999). However, Fgf10 also binds with high affinity to Fgfr1b (Ornitz et al., 1996) that is expressed by both the epithelium and mesenchyme (Lee et al., 2008). In the early developing mouse lung, it is well accepted that mesenchymal Fgf10 acts on the epithelium through its receptor Fgfr2b, while direct action on the mesenchyme does not occur until E14.5 (De Langhe et al., 2006). Our results suggest that during late lung development, Fgf10 signals to the mesenchyme through both Fgfr2b and Fgfr1b and that the two receptors play redundant roles in terms of LIF formation. The expression of *Fgfr2b* in the lung mesenchyme is a novel finding that suggests a mechanism of alternative splicing to allow the expression of this receptor. In the future, it will be interesting to investigate what controls *Fgfr2b* expression in the mesenchyme. The generation of double conditional knock out of *Fgfr1b/2b* in the mesenchyme will also be important to clarify whether these two receptors are the only mediators of Fgf10 signaling in the lung mesenchyme.

Can Fgf10-regulated epithelial signals also contribute to the formation of lipofibroblasts during development?

The current work shows clearly that Fgf10 acts directly on the mesenchyme, and that Fgfr1b and 2b likely play redundant roles as receptors for Fgf10. However, Fgf10 also acts on the distal epithelial progenitor cells expressing *Fgfr2b* throughout lung development. Therefore, it is possible that some of the effects observed upon reduction of *Fgf10* levels, or upon inhibition of the Fgfr2b ligand activity, may result from the loss of epithelial-derived signals that would also impact LIF formation. We also investigated the expression levels of *Sftpc* and *Scgb1a1* in the various mutants by qPCR (Fig. S3). *Sftpc* expression levels were significantly reduced in Fgfr2b attenuation (Fig. S3A; $P<0.001$) and *Fgf10* hypomorphic lungs (Fig. S3C; $P<0.01$) but not in *Fgfr1b* knockout (Fig. S3E) or *Fgfr2b* conditional knockout lungs (Fig. S3G) compared to littermate controls. *Scgb1a1* expression levels did not display significant changes in any of these mutants (Fig. S3B,D,F,H). In the future, the possible involvement of epithelial-derived signals in LIF formation upon the

manipulation of Fgf10 signaling can be tested by knocking out *Fgfr1b* and *Fgfr2b* in the lung epithelium (specifically in Sftpc^{+} cells) at E14.5 and examining LIF formation at E18.5.

In conclusion, our findings identify, for the first time the developmental heterogeneity of pulmonary LIFs and specifically describe the *Fgf10*-positive LIF subpopulation. We demonstrate that Fgf10 signals in an autocrine/paracrine fashion to promote the formation of LIFs, likely through Pparg activation. Our data from human fetal tissues and cells suggest that the role of Fgf10 signaling in LIF formation in mice can be extrapolated to humans. *Fgf10*-positive cells and LIFs represent important understudied cell populations in the lung that may be crucial for the repair process after injury during adult life.

Materials and Methods

Ethics statement: Human fetal biopsies at different gestational ages were obtained under IRB approval CHLA-14-2211. Exclusion criteria are HIV and Hepatitis. All the samples used in this study had no known genetic abnormalities.

Animal experiments were performed under the research protocol approved by the Animal Research Committee at Children's Hospital Los Angeles and Labiomed at Harbor UCLA and in strict accordance with the recommendations in the Guide for the Care and Use of Laboratory Animals of the National Institutes of Health. The approval identification for Children's Hospital Los Angeles is AAALAC A3276-01 (protocols 31-08 and 253-11). Mouse protocols were also approved by Justus Liebig University Giessen (Approval numbers 405_M, 437_M and 452_M).

Mice: The *Rosa26*$^{rTtA/+}$*; tet(O)sFgfr2b/+* double heterozygous mice were previously described (Parsa et al., 2008). To attenuate Fgfr2b ligands, pregnant females carrying double transgenic (DTG) embryos and single transgenic littermate controls were put on a doxycycline-containing diet (normal rodent diet with 0.0625% doxycycline, Harlan Teklad). For lineage tracing and sorting of *Fgf10*-positive cells, we used *Fgf10*^{iCre} mice crossed with *Tomato*$^{flox/flox}$ reporter mice as previously described (El Agha et al., 2012; El Agha et al., 2014). Females carrying *Fgf10*^{iCre}; *tomato*$^{flox/+}$ embryos received two IP injections of tamoxifen (0.1 mg/g of body weight each) at E11.5 and E14.5, and lungs were collected at E18.5. In order to perform lineage tracing in the context of *Fgf10* hypomorph, *Fgf10*$^{iCre/+}$*; tomato*$^{flox/flox}$ mice were crossed with *Fgf10-lacZ/+* mice (Kelly et al., 2001) to generate *Fgf10*$^{iCre/+}$*; tomato*$^{flox/+}$ (control) and *Fgf10*$^{iCre/lacZ}$*; tomato*$^{flox/+}$ (hypomorph) embryos. The *Fgf10*^{iCre} allele corresponds to a loss of function allele for *Fgf10* (El Agha et al., 2012) whereas the *Fgf10-lacZ* allele is a hypomorphic allele for *Fgf10* (Ramasamy et al., 2007).

X-gal staining: LacZ staining of post-natal *Fgf10-lacZ* lungs was performed as previously described (Al Alam et al., 2011).

FACS sorting: Lungs from E18.5 *Fgf10*^{iCre}*; tomato*$^{flox/+}$ embryos were dissected in HBSS on ice, put into a mixture of 0.5% collagenase/DNase in HBSS, cut into small pieces then incubated for 30 min at 37°C under vigorous shaking. The cells were then

strained through 100 µm followed by 40 µm cell strainers, washed and counted. Cells were stained with CD45 for 30 min on ice to exclude blood cells. The endogenous Tomato signal was detected using the PE channel. DAPI was used to exclude dead cells. The analyses and sorting were performed using a FACSAria III cell sorter and the FACS Diva version 6.1.3. Gates were set according to unstained controls.

Histology: After fixation in 4% PFA, lungs were washed in PBS, dehydrated in graded ethanol solutions, cleared in xylene and embedded in paraffin. For immunostaining, 5-micron sections were cleared twice with xylene and re-hydrated, equilibrated in water and then washed in PBS. Antigen retrieval was performed in citrate buffer (pH 6) at 95°C for 15 min. Hematoxylin and eosin (H&E) staining was done according to standard procedures. For immunostaining, slides were incubated with primary antibodies against Acta2 (Dako cytomation), Cdh1 (BD Biosciences), Sftpc (Seven Hills) and Adrp (Abcam) at 4°C overnight. For Adrp immunofluorescence staining (IF), FITC-conjugated secondary antibodies (Jackson Laboratories) were used. MetaMorph software (Leica Microsystems) was used for quantifying Adrp immunoreactive spots (count and size). Three to four 40x fields per sample were analyzed. Oil red O (ORO) staining was performed as previously described (Rehan and Torday, 2003; Rehan et al., 2007; Rehan et al., 2006). Immunohistochemistry (IHC) was performed with Dako EnVision kit according to the manufacturer's instructions. Fluorescence images were acquired using a Leica monocolor camera attached to a Leica DM4000B microscope. Bright field and DIC images were acquired on using AxioCam MRc color CCD camera (Zeiss Microimaging, Thornwood, NY).

Primary culture of lung fibroblasts and WI-38 cell line: Whole lungs were dissected from embryos, minced into small pieces and then subjected to 0.025% trypsin (20 min at 37°C for rat lungs) or 0.5% collagenase IV (45 min at 37°C for mouse lungs) digestion to give rise to single cells. Mesenchymal cells were separated from epithelial cells by differential adhesion as described previously (Lebeche et al., 1999). Thirty minutes after plating, floating cells and media were removed and adherent cells were washed several times with PBS. Human embryonic fibroblast cell line WI-38 was cultured in presence or absence of different concentrations of recombinant human (rh)FGF10 (0; 1; 10; 100; 250 ng/mL) (R&D Systems).

Isolation of fetal human lung cells: Human distal lung pieces, cut at 1 mm from the edge of 16 weeks gestational age specimen, were placed into a Miltenyi C-tube and incubated at 37°C for 10 min with an enzyme mix from the Miltenyi human tumor dissociation kit. The dissociation was then completed using the gentleMACS dissociator. After wash and red blood cell lysis, the cell suspensions were filtered on 40 µm filter, counted and blocked with Fc fragments for 15 min. Following blocking, the cells were incubated with anti-CD45 microbeads, eluted through the column to exclude the CD45+ cells. The remaining cells were incubated with anti-CD326 microbeads to positively select for epithelial cells. After elution, the CD326+ cells were flushed from the magnetic column. The remaining fraction depleted of CD45 and CD326, was then incubated with anti-CD31 microbeads, in order to obtain an endothelial-free mesenchymal fraction. RNA was extracted from the epithelial fraction and the final mesenchymal fraction depleted of CD31.

Gene expression analyses: RNA extracted from lung tissues or cells was reverse-transcribed into cDNA using Transcriptor High Fidelity cDNA Synthesis Kit (Roche Applied Science) according to the manufacturer's instructions. cDNA was used for dual color Hydrolysis Probe – Universal probe library-based quantitative real-time PCR (qPCR), using the LightCycler 480 from Roche Applied Science. Primers were designed using Roche Applied Science probe-based assay design center. *Gapdh* assay, commercially available from Roche Applied Science, was used as the reference gene.

Western blotting: Whole lungs or cultured lung mesenchymal cells were disrupted immediately in RIPA buffer containing protease inhibitors. Equal amounts of total lung protein (50 µg) from each assayed sample were used for chemiluminescent western analysis (Roche Molecular Biochemicals) on immunoblot PVDF membranes (Bio-Rad, Hercules, CA). Immunoblotting was performed using antibodies against PPARγ (Santa Cruz, sc-7196) and GAPDH (Chemicon, MAb 374).

Triolein uptake: Triolein uptake by the LIFs was performed as previously described (Karadag et al., 2009). Briefly, lung tissues were minced into small pieces and incubated with [3H]triolein (5 µCi/mL) in DMEM supplemented with 20% rat serum. The tissue pieces were then washed twice with 1 mL of ice cold PBS and homogenized, a portion of which was used for protein extraction and the remainder for neutral lipid content.

Statistical analyses: Statistical analyses were performed using GraphPad Prism software. Non-parametric tests were used to compare two groups and one way-ANOVA was used to compare multiple groups. Data are presented as average values ± s.e.m. The results were considered significant if $P<0.05$.

Acknowledgements

SB, EEA, JQ, CS and SH acknowledge the support from the German Lung center for lung research, the Excellence Cluster Cardio-Pulmonary System, the UKGM and the Universities of Giessen and Marburg Lung Center. SB acknowledges the support from the Landes-Offensive zur Entwicklung wissenschaftlich-ökonomischer Exzellenz and Deutsche Forschungsgemeinschaft (projects BE 4443/1-1 and BE 443/4-1), the NIH/NHLBI (1R01HL086322-01A2), COST BM1201 as well as the program of competitive growth of Kazan Federal University. JQ, CS and SH also acknowledge the Deutsche Forschungsgemeinschaft (project SFB1021 C05). VKR acknowledges the support of the NIH (RO1HD051857, R21HD071731 and R21HL107118). DAL acknowledges the support of ALA (RTF09) and AHA (11POST7440038). PM is Hastings Professor of Pediatrics and acknowledges the support of NIH/NHLBI (HL107307). SDL acknowledges the support of NIH/NHLBI (R01HL092967), March of Dimes (1-FY15-352) and the pulmonary fibrosis foundation (The Albert Rose established investigator award). MVP acknowledges support of the Edward Mallinckrodt Jr. Foundation Research Grant and NIH/NIAMS (R01AR067273). We thank Salma Dilai for her help with MetaMorph software. We would like to thank also Drs. Melissa L. Wilson (University of Southern California, Department of Preventive Medicine) and Rachel Steward (University of Southern California, Department of Obstetrics and Gynecology) for coordinating the efforts to obtain human fetal lungs.

Authors contribution

SB , DAA, EEA, SDL, PM, VR, developed the concepts or approach,. DAA, EEA, RS, VK, AM, SD , AS, CS, JQ, CMC, SDL, MT, BG, SB performed experiments or data analysis, and SB , DAA, EEA, SH, CT, SDL, MP, PM, VR prepared or edited the manuscript prior to submission.

References

Al Alam, D., Green, M., Tabatabai Irani, R., Parsa, S., Danopoulos, S., Sala, F.G., Branch, J., El Agha, E., Tiozzo, C., Voswinckel, R., Jesudason, E.C., Warburton, D., Bellusci, S., 2011. Contrasting expression of canonical Wnt signaling reporters TOPGAL, BATGAL and Axin2(LacZ) during murine lung development and repair. PLoS One 6, e23139.

Asaki, T., Konishi, M., Miyake, A., Kato, S., Tomizawa, M., Itoh, N., 2004. Roles of fibroblast growth factor 10 (Fgf10) in adipogenesis in vivo. Mol Cell Endocrinol 218, 119-128.

Barkauskas, C.E., Cronce, M.J., Rackley, C.R., Bowie, E.J., Keene, D.R., Stripp, B.R., Randell, S.H., Noble, P.W., Hogan, B.L., 2013. Type 2 alveolar cells are stem cells in adult lung. J Clin Invest 123, 3025-3036.

Bellusci, S., Grindley, J., Emoto, H., Itoh, N., Hogan, B.L., 1997. Fibroblast growth factor 10 (FGF10) and branching morphogenesis in the embryonic mouse lung. Development 124, 4867-4878.

Berry, R., Rodeheffer, M.S., 2013. Characterization of the adipocyte cellular lineage in vivo. Nat Cell Biol 15, 302-308.

De Langhe, S.P., Carraro, G., Warburton, D., Hajihosseini, M.K., Bellusci, S., 2006. Levels of mesenchymal FGFR2 signaling modulate smooth muscle progenitor cell commitment in the lung. Dev Biol 299, 52-62.

De Moerlooze, L., Spencer-Dene, B., Revest, J.M., Hajihosseini, M., Rosewell, I., Dickson, C., 2000. An important role for the IIIb isoform of fibroblast growth factor receptor 2 (FGFR2) in mesenchymal-epithelial signalling during mouse organogenesis. Development 127, 483-492.

El Agha, E., Al Alam, D., Carraro, G., MacKenzie, B., Goth, K., De Langhe, S.P., Voswinckel, R., Hajihosseini, M.K., Rehan, V.K., Bellusci, S., 2012. Characterization of a novel fibroblast growth factor 10 (Fgf10) knock-in mouse line to target mesenchymal progenitors during embryonic development. PLoS One 7, e38452.

El Agha, E., Bellusci, S., 2014. Walking along the Fibroblast Growth Factor 10 Route: A Key Pathway to Understand the Control and Regulation of Epithelial and Mesenchymal Cell-Lineage Formation during Lung Development and Repair after Injury. Scientifica 2014, 538379.

El Agha, E., Herold, S., Al Alam, D., Quantius, J., MacKenzie, B., Carraro, G., Moiseenko, A., Chao, C.M., Minoo, P., Seeger, W., Bellusci, S., 2014. Fgf10-positive cells represent a progenitor cell population during lung development and postnatally. Development 141, 296-306.

Ferguson, H.E., Thatcher, T.H., Olsen, K.C., Garcia-Bates, T.M., Baglole, C.J., Kottmann, R.M., Strong, E.R., Phipps, R.P., Sime, P.J., 2009. Peroxisome proliferator-activated receptor-gamma ligands induce heme oxygenase-1 in lung fibroblasts by a PPARgamma-independent, glutathione-dependent mechanism. American journal of physiology. Lung cellular and molecular physiology 297, L912-919.

Jonker, J.W., Suh, J.M., Atkins, A.R., Ahmadian, M., Li, P., Whyte, J., He, M., Juguilon, H., Yin, Y.Q., Phillips, C.T., Yu, R.T., Olefsky, J.M., Henry, R.R., Downes, M., Evans, R.M., 2012. A PPARgamma-FGF1 axis is required for adaptive adipose remodelling and metabolic homeostasis. Nature 485, 391-394.

Kaplan, N.B., Grant, M.M., Brody, J.S., 1985. The lipid interstitial cell of the pulmonary alveolus. Age and species differences. Am Rev Respir Dis 132, 1307-1312.
Karadag, A., Sakurai, R., Wang, Y., Guo, P., Desai, M., Ross, M.G., Torday, J.S., Rehan, V.K., 2009. Effect of maternal food restriction on fetal rat lung lipid differentiation program. Pediatr Pulmonol 44, 635-644.
Kelly, R.G., Brown, N.A., Buckingham, M.E., 2001. The arterial pole of the mouse heart forms from Fgf10-expressing cells in pharyngeal mesoderm. Dev Cell 1, 435-440.
Konishi, M., Asaki, T., Koike, N., Miwa, H., Miyake, A., Itoh, N., 2006. Role of Fgf10 in cell proliferation in white adipose tissue. Mol Cell Endocrinol 249, 71-77.
Lebeche, D., Malpel, S., Cardoso, W.V., 1999. Fibroblast growth factor interactions in the developing lung. Mech Dev 86, 125-136.
Lee, J.M., Kim, J.Y., Cho, K.W., Lee, M.J., Cho, S.W., Kwak, S., Cai, J., Jung, H.S., 2008. Wnt11/Fgfr1b cross-talk modulates the fate of cells in palate development. Dev Biol 314, 341-350.
Mailleux, A.A., Kelly, R., Veltmaat, J.M., De Langhe, S.P., Zaffran, S., Thiery, J.P., Bellusci, S., 2005. Fgf10 expression identifies parabronchial smooth muscle cell progenitors and is required for their entry into the smooth muscle cell lineage. Development 132, 2157-2166.
Mailleux, A.A., Spencer-Dene, B., Dillon, C., Ndiaye, D., Savona-Baron, C., Itoh, N., Kato, S., Dickson, C., Thiery, J.P., Bellusci, S., 2002. Role of FGF10/FGFR2b signaling during mammary gland development in the mouse embryo. Development 129, 53-60.
McCulley, D., Wienhold, M., Sun, X., 2015. The pulmonary mesenchyme directs lung development. Current opinion in genetics & development 32, 98-105.
McGowan, S.E., McCoy, D.M., 2015. Fibroblast growth factor signaling in myofibroblasts differs from lipofibroblasts during alveolar septation in mice. American journal of physiology. Lung cellular and molecular physiology 309, L463-474.
McGowan, S.E., Torday, J.S., 1997. The pulmonary lipofibroblast (lipid interstitial cell) and its contributions to alveolar development. Annu Rev Physiol 59, 43-62.
McIntosh, J.C., Hagood, J.S., Richardson, T.L., Simecka, J.W., 1994. Thy1 (+) and (-) lung fibrosis subpopulations in LEW and F344 rats. Eur Respir J 7, 2131-2138.
McQualter, J.L., Bertoncello, I., 2012. Concise review: Deconstructing the lung to reveal its regenerative potential. Stem cells 30, 811-816.
O'Hare, K.H., Sheridan, M.N., 1970. Electron microscopic observations on the morphogenesis of the albino rat lung, with special reference to pulmonary epithelial cells. Am J Anat 127, 181-205.
Ohta, H., Itoh, N., 2014. Roles of FGFs as Adipokines in Adipose Tissue Development, Remodeling, and Metabolism. Frontiers in endocrinology 5, 18.
Ornitz, D.M., Xu, J., Colvin, J.S., McEwen, D.G., MacArthur, C.A., Coulier, F., Gao, G., Goldfarb, M., 1996. Receptor specificity of the fibroblast growth factor family. J Biol Chem 271, 15292-15297.
Parsa, S., Kuremoto, K., Seidel, K., Tabatabai, R., Mackenzie, B., Yamaza, T., Akiyama, K., Branch, J., Koh, C.J., Al Alam, D., Klein, O.D., Bellusci, S., 2010. Signaling by FGFR2b controls the regenerative capacity of adult mouse incisors. Development 137, 3743-3752.

Parsa, S., Ramasamy, S.K., De Langhe, S., Gupte, V.V., Haigh, J.J., Medina, D., Bellusci, S., 2008. Terminal end bud maintenance in mammary gland is dependent upon FGFR2b signaling. Dev Biol 317, 121-131.
Penney, D.P., Keng, P.C., Derdak, S., Phipps, R.P., 1992. Morphologic and functional characteristics of subpopulations of murine lung fibroblasts grown in vitro. Anat Rec 232, 432-443.
Phipps, R.P., Baecher, C., Frelinger, J.G., Penney, D.P., Keng, P., Brown, D., 1990. Differential expression of interleukin 1 alpha by Thy-1+ and Thy-1- lung fibroblast subpopulations: enhancement of interleukin 1 alpha production by tumor necrosis factor-alpha. Eur J Immunol 20, 1723-1727.
Ramasamy, S.K., Mailleux, A.A., Gupte, V.V., Mata, F., Sala, F.G., Veltmaat, J.M., Del Moral, P.M., De Langhe, S., Parsa, S., Kelly, L.K., Kelly, R., Shia, W., Keshet, E., Minoo, P., Warburton, D., Bellusci, S., 2007. Fgf10 dosage is critical for the amplification of epithelial cell progenitors and for the formation of multiple mesenchymal lineages during lung development. Dev Biol 307, 237-247.
Rehan, V., Torday, J., 2003. Hyperoxia augments pulmonary lipofibroblast-to-myofibroblast transdifferentiation. Cell Biochem Biophys 38, 239-250.
Rehan, V.K., Sakurai, R., Wang, Y., Santos, J., Huynh, K., Torday, J.S., 2007. Reversal of nicotine-induced alveolar lipofibroblast-to-myofibroblast transdifferentiation by stimulants of parathyroid hormone-related protein signaling. Lung 185, 151-159.
Rehan, V.K., Sugano, S., Wang, Y., Santos, J., Romero, S., Dasgupta, C., Keane, M.P., Stahlman, M.T., Torday, J.S., 2006. Evidence for the presence of lipofibroblasts in human lung. Exp Lung Res 32, 379-393.
Rubin, L.P., Kovacs, C.S., De Paepe, M.E., Tsai, S.W., Torday, J.S., Kronenberg, H.M., 2004. Arrested pulmonary alveolar cytodifferentiation and defective surfactant synthesis in mice missing the gene for parathyroid hormone-related protein. Dev Dyn 230, 278-289.
Sakaue, H., Konishi, M., Ogawa, W., Asaki, T., Mori, T., Yamasaki, M., Takata, M., Ueno, H., Kato, S., Kasuga, M., Itoh, N., 2002. Requirement of fibroblast growth factor 10 in development of white adipose tissue. Genes Dev 16, 908-912.
Schultz, C.J., Torres, E., Londos, C., Torday, J.S., 2002. Role of adipocyte differentiation-related protein in surfactant phospholipid synthesis by type II cells. American journal of physiology. Lung cellular and molecular physiology 283, L288-296.
Sekine, K., Ohuchi, H., Fujiwara, M., Yamasaki, M., Yoshizawa, T., Sato, T., Yagishita, N., Matsui, D., Koga, Y., Itoh, N., Kato, S., 1999. Fgf10 is essential for limb and lung formation. Nat Genet 21, 138-141.
Simon, D.M., Mariani, T.J., 2007. Role of PPARs and Retinoid X Receptors in the Regulation of Lung Maturation and Development. PPAR Res 2007, 91240.
Torday, J.S., Torres, E., Rehan, V.K., 2003. The role of fibroblast transdifferentiation in lung epithelial cell proliferation, differentiation, and repair in vitro. Pediatr Pathol Mol Med 22, 189-207.
Tordet, C., Marin, L., Dameron, F., 1981. Pulmonary di-and-triacylglycerols during the perinatal development of the rat. Experientia 37, 333-334.
Tran, K.V., Gealekman, O., Frontini, A., Zingaretti, M.C., Morroni, M., Giordano, A., Smorlesi, A., Perugini, J., De Matteis, R., Sbarbati, A., Corvera, S., Cinti, S., 2012. The vascular endothelium of the adipose tissue gives rise to both white and brown fat cells. Cell Metab 15, 222-229.

Varisco, B.M., Ambalavanan, N., Whitsett, J.A., Hagood, J.S., 2012. Thy-1 signals through PPARgamma to promote lipofibroblast differentiation in the developing lung. Am J Respir Cell Mol Biol 46, 765-772.
Volckaert, T., Dill, E., Campbell, A., Tiozzo, C., Majka, S., Bellusci, S., De Langhe, S.P., 2011. Parabronchial smooth muscle constitutes an airway epithelial stem cell niche in the mouse lung after injury. J Clin Invest 121, 4409-4419.

Figures

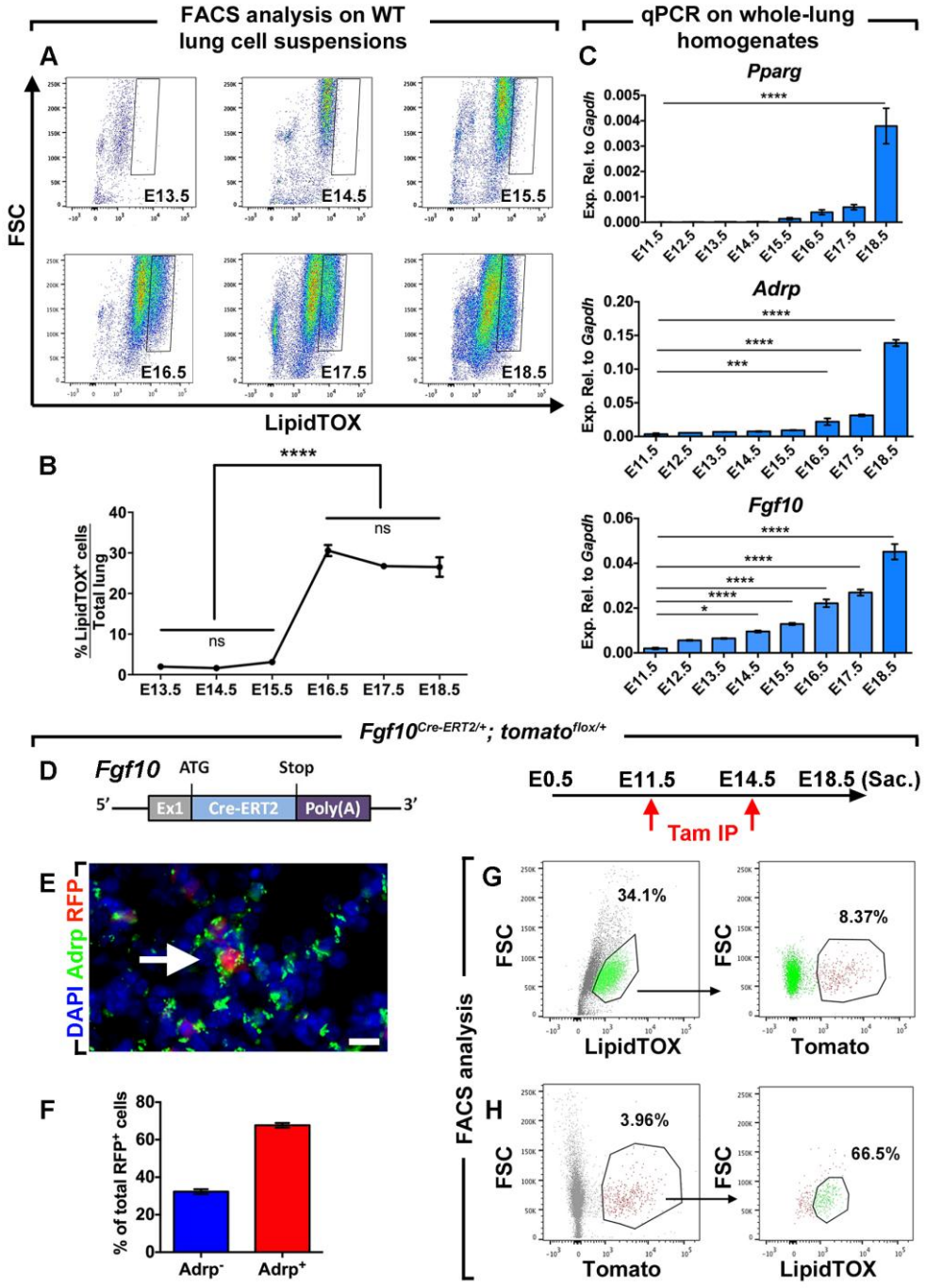

Figure 1: Lipofibroblasts emerge in the mouse lung during late pseudoglandular stage. (A) FACS analysis of LipidTOX-stained cell suspensions from embryonic CD1 lungs. Note the sudden increase in LipidTOX^{+} cells between E15.5 and E16.5. **(B)**

Quantification of the FACS plots shown in (A) (*n*=4 per stage). **(C)** qPCR analysis showing the expression patterns of *Fgf10*, *Pparg* and *Adrp* during embryonic lung development (*n*=3 per stage). **(D)** Schematic representation of the *Fgf10*^{iCre} mouse construct and the time line of tamoxifen treatment and embryo harvest. **(E)** IF for Adrp (green). The endogenous Tomato signal was detected using the RFP channel (red). The arrow indicates an Adrp^{+} RFP^{+} cell. **(F)** Quantification of IF shown in (E). **(G)** FACS analysis showing that RFP^{+} cells represent 8.37% of total LipidTOX^{+} cells. **(H)** FACS analysis showing that 66.5% of RFP^{+} cells are also LipidTOX^{+}. Scale bar: 10 µm. * *P*<0.05, *** *P*<0.001, **** *P*<0.0001. Tam IP: intraperitoneal injection of tamoxifen.

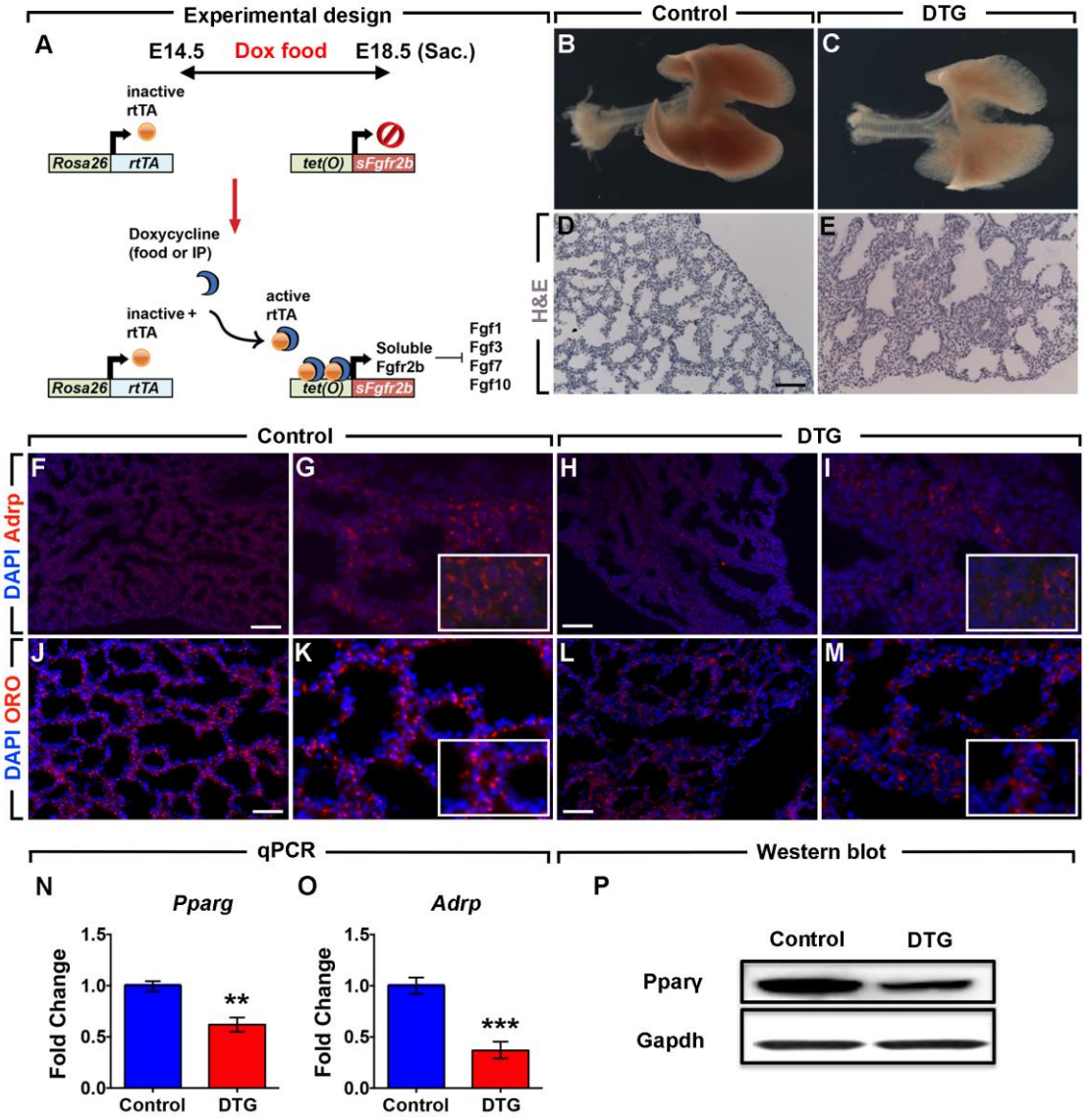

Figure 2: Attenuation of *Fgfr2b* ligand activity leads to impaired LIF formation. **(A)** Inducible mouse model used to overexpress the soluble form of *Fgfr2b* receptor acting as a decoy receptor for Fgfr2b ligands between E14.5 to E18.5. **(B,C)** Whole mount views of control (B) and DTG (C) lungs. **(D,E)** H&E staining of control (E) and DTG (F) lung sections. **(F)** IF for Adrp in control lungs. **(G)** High magnification of (F). The inset in (G) shows a higher magnification. **(H)** IF for Adrp in DTG lungs. **(I)** High magnification of (H). The inset in (I) shows a higher magnification. **(J)** ORO staining of frozen sections from control lungs. **(K)** High magnification of (J). The inset in (K) shows a higher magnification. **(L)** ORO staining of frozen sections from DTG lungs. **(M)** High magnification of (L). The inset in (M) shows a higher

magnification. **(N,O)** qPCR for *Pparg* and *Adrp* showing decreased expression levels in DTG lungs compared to control lungs. **(P)** Western blot showing reduction in Pparg expression in DTG lungs compared to control lungs. Scale bars: (D,J,L) 50 µm, (F,H) 100 µm. *n*=4 per group. ** *P*<0.01, *** *P*<0.001. DTG: Double transgenic.

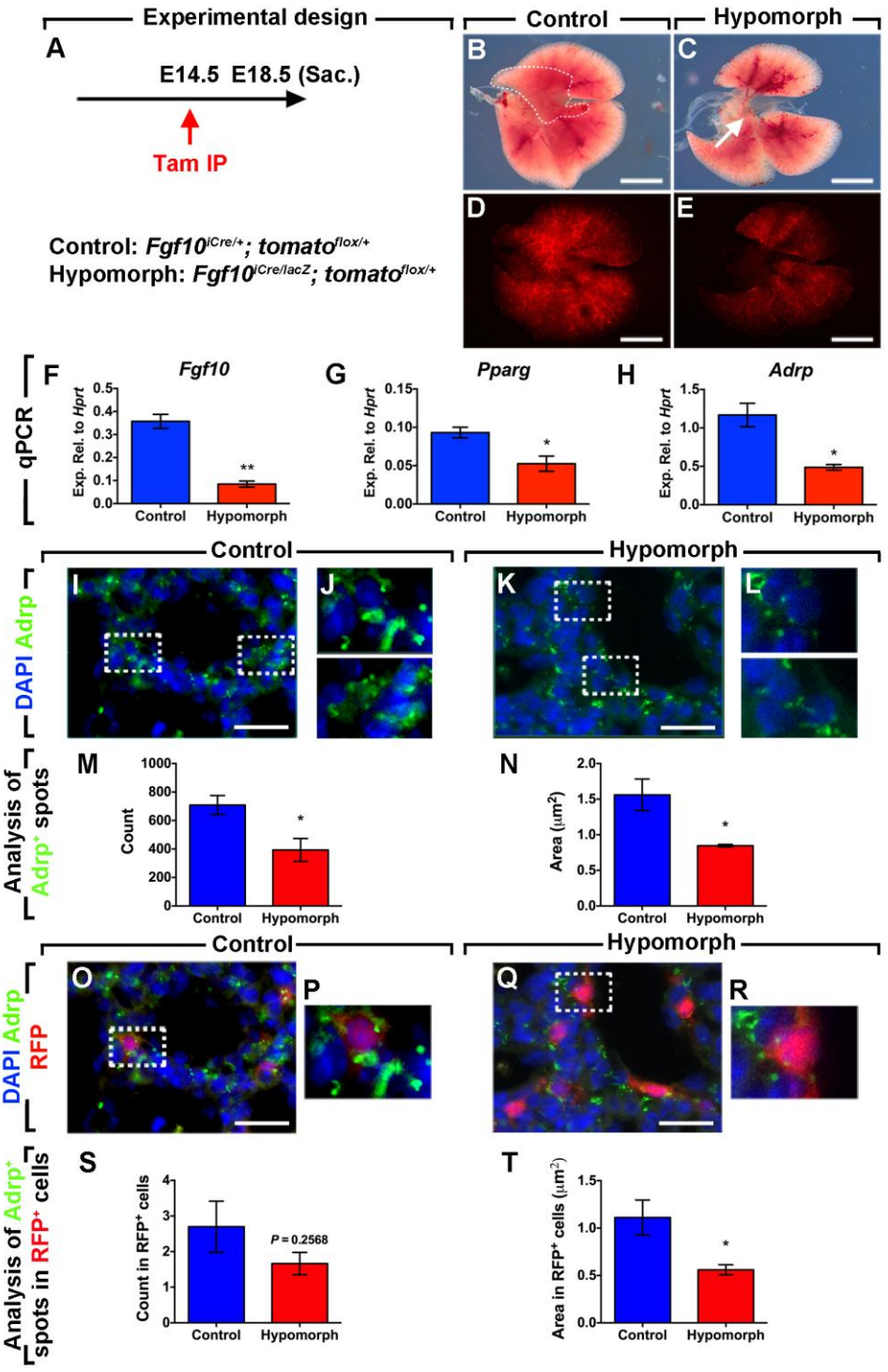

Figure 3: *Fgf10* hypomorphs exhibit impaired LIF formation. (A) Experimental design showing the time line of tamoxifen treatment and tissue harvest. The control and hypomorphic genotypes are shown. **(B,C)** Whole mount views of control and hypomorphic E18.5 lungs. Note the absence of the accessory lobe in the hypomorph. **(D,E)** Whole mount fluorescent images of the lungs showing Tomato expression. **(F-**

H) qPCR analysis showing decreased expression of *Fgf10*, *Pparg* and *Adrp* in the hypomorphic lungs compared to control lungs. **(I)** IF for Adrp in control lungs. **(J)** High magnification of two fields from (I). **(K)** IF for Adrp in hypomorphic lungs. **(L)** High magnification of two fields from (K). **(M,N)** Quantification of Adrp immunoreactivity shown in (I-L) using MetaMorph software. **(O)** IF for Adrp in control lungs showing Tomato expression. **(P)** High magnification of (O). **(Q)** IF for Adrp in hypomorphic lungs showing Tomato expression. **(R)** High magnification of (Q). **(S,T)** Quantification of Adrp immunoreactivity in the lineage-labeled cells shown in (O-R). Scale bars: (B-E) 750 μm, (I,K,O,Q) 25 μm. n=3 per group. * P<0.05, ** P<0.01.

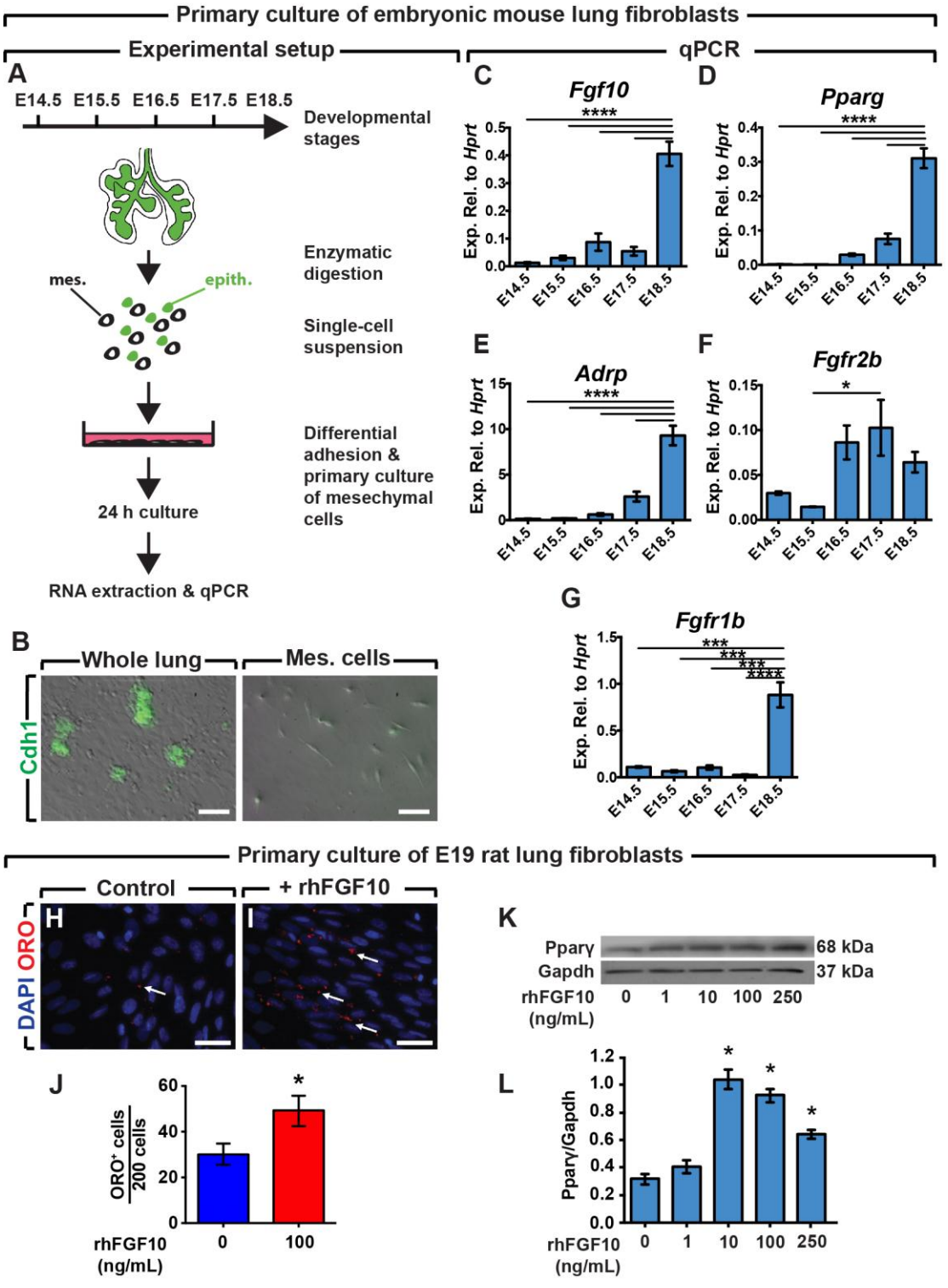

Figure 4: Fgf10 acts directly on mesenchymal cells. (A) Time line for harvesting embryonic lungs and the subsequent experimental plan. **(B)** IF for Cdh1 showing minimal epithelial contamination in the primary culture of embryonic lung mesenchyme. **(C-G)** qPCR analysis for *Fgf10*, *Pparg*, *Adrp*, *Fgfr2b* and *Fgfr1b*. **(H)**

ORO staining of control and rhFGF10-treated primary E19 rat lung fibroblasts. Note the increase in the number of ORO^+ cells in rhFGF10-treated cells (white arrows). **(J)** Quantification of the ORO signal shown in (H,I). (K) Western blot showing upregulation of Pparg upon treatment with increasing concentrations of rhFGF10 (1-250 ng/mL). (L) Densitometric analysis of the Western blot data shown in (K). Scale bars: (B) 50 µm, (H,I) 25 µm. $3 \leq n \leq 6$. * $P<0.05$, **** $P<0.0001$. Mes: mesenchyme.

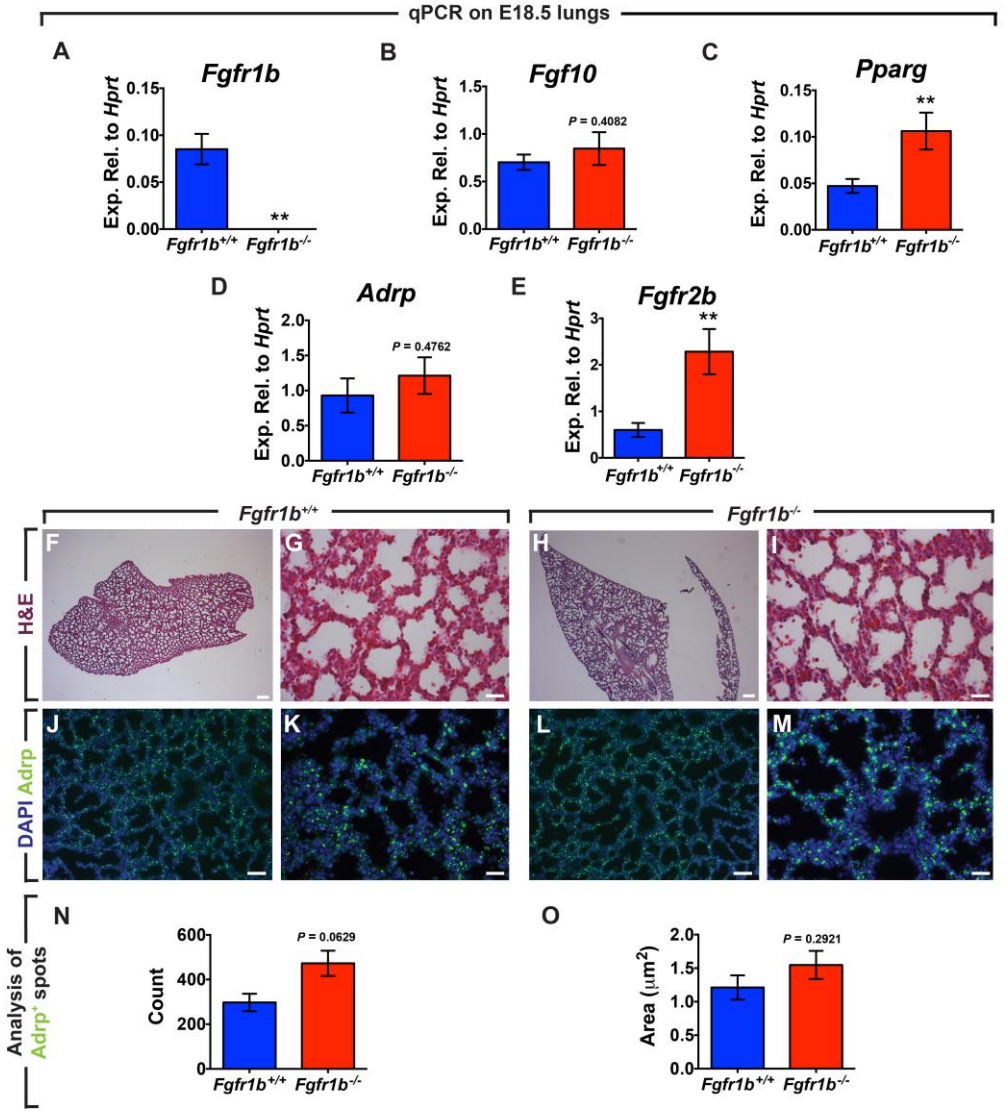

Figure 5: *Fgfr1b* knockouts suggest compensation with Fgfr2b. (A-E) qPCR analysis of *Fgfr1b*, *Fgf10*, *Pparg*, *Adrp* and *Fgfr2b* in *Fgfr1b*$^{-/-}$ lungs compared to littermate controls. **(F-I)** H&E staining showing no apparent histological differences between control (F,G) and *Fgfr1b* knockout lungs (H,I). **(J-M)** IF for Adrp showing a slight increase in immunoreactivity in *Fgfr1b* knockout lungs (L,M) compared to control lungs (J,K). **(N,O)** Quantification of Adrp immunoreactivity using MetaMorph software. Scale bars: (F,H) 200 μm, (G,I,K,M) 25 μm; (J,L) 50 μm. (A-E) *Fgfr1b*$^{+/+}$: *n*=7, *Fgfr1b*$^{-/-}$: *n*=4. (N,O): *Fgfr1b*$^{+/+}$: *n*=3, *Fgfr1b*$^{-/-}$: *n*=3. ** *P*<0.01.

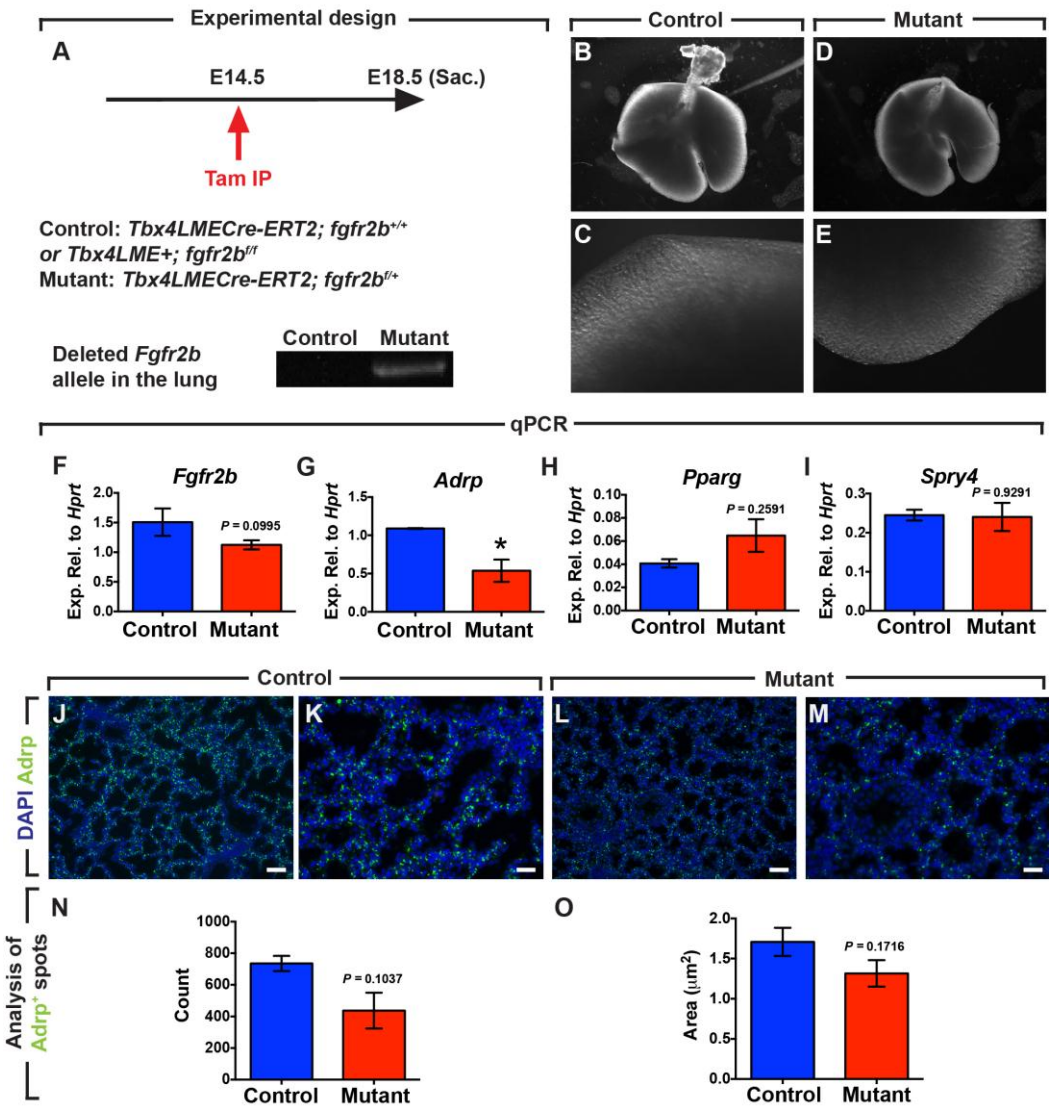

Figure 6: Conditional deletion of *Fgfr2b* in the lung mesenchyme mildly impairs lipofibroblast formation. (A) Schematic representation of the time line of tamoxifen treatment and tissue harvest. Control and mutant genotypes are defined and the detection of the deleted *Fgfr2b* allele is also shown. **(B-E)** Whole-mount view of control and mutant lungs showing no apparent phenotype. **(F-I)** qPCR analysis showing a trend towards decreased *Fgfr2b*, a statistically significant decrease in *Adrp* and unchanged *Pparg* and *Spry4* expression levels in mutant lungs compared to control lungs. **(J-M)** IF for Adrp showing a slight decrease in immunoreactivity in mutant lungs (L,M) compared to control lungs (J,K). **(N,O)** Quantification of Adrp immunoreactivity using MetaMorph software. Scale bars: (J,L) 50 µm, (K,M) 25 µm. n=3 for controls and n=5 for mutants. * P<0.05.

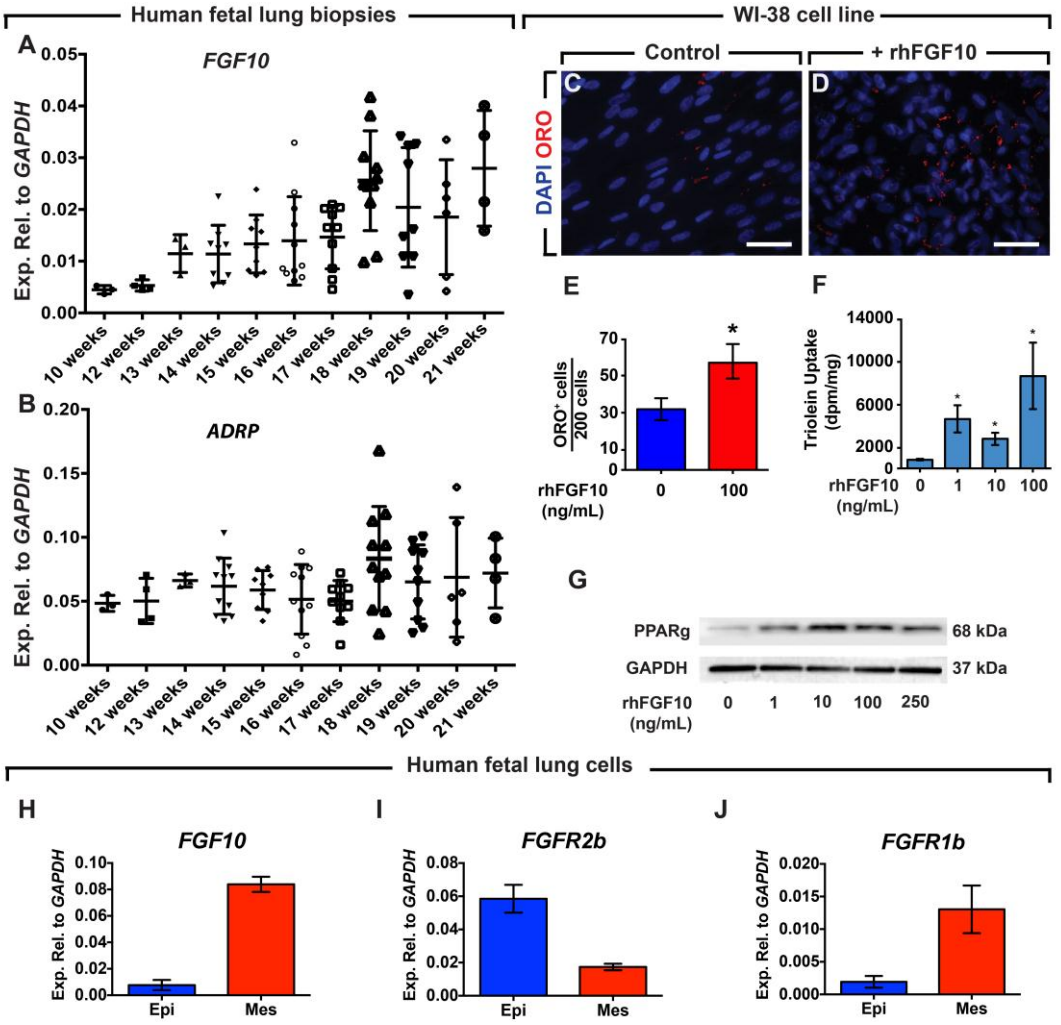

Figure 7. FGF10 promotes lipofibroblast formation in human mesenchyme. (A,B) Expression levels of *FGF10* and *ADRP* in human fetal lungs. **(C,D)** ORO staining of untreated and rhFGF10-treated WI-38 cells. The increase in ORO^{+} cells is quantified in **(E)**. **(F)** Triolein uptake measured in protein extracts from WI-38 cells cultured for 24 hours with serum-free media in absence or presence of rhFGF10 (1, 10 and 100 ng/mL). **(G)** Western blot for PPARg and GAPDH in WI-38 cells cultured for 24 hours with serum-free media in absence or presence of rhFGF10. (H-I) qPCR for *FGF10, FGFR2b* and *FGFR1b* in epithelial and mesenchymal cells isolated from 16 weeks gestational age human lungs. Scale bars: 25 µm. (A,B): $3 \leq n \leq 11$, (E-G): $n=3$, (H-J): $n=2$ per group. * $P<0.05$.